

Article

Electric Transport in Few-Layer ReSe₂ Transistors Modulated by Air Pressure and Light

Enver Faella ^{1,2}, Kimberly Intonti ¹, Loredana Viscardi ¹, Filippo Giubileo ², Arun Kumar ¹, Hoi Tung Lam ³, Konstantinos Anastasiou ³, Monica F. Craciun ³, Saverio Russo ³ and Antonio Di Bartolomeo ^{1,2,*}

¹ Department of Physics “E.R. Caianiello”, University of Salerno, 84084 Fisciano, SA, Italy; efaella@unisa.it (E.F.); k.intonti@studenti.unisa.it (K.I.); l.viscardi7@studenti.unisa.it (L.V.); akumar@unisa.it (A.K.)

² CNR-SPIN, 84084 Fisciano, SA, Italy; filippo.giubileo@spin.cnr.it

³ University of Exeter, Stocker Road 6, Exeter EX4 4QL, Devon, UK; o.lam@exeter.ac.uk (H.T.L.); ka391@exeter.ac.uk (K.A.); m.f.craciun@exeter.ac.uk (M.F.C.); s.russo@exeter.ac.uk (S.R.)

* Correspondence: adibartolomeo@unisa.it; Tel.: +39-089-96-9189

Abstract: We report the fabrication and optoelectronic characterization of field-effect transistors (FETs) based on few-layer ReSe₂. The devices show n-type conduction due to the Cr contacts that form low Schottky barriers with the ReSe₂ nanosheet. We show that the optoelectronic performance of these FETs is strongly affected by air pressure, and it undergoes a dramatic increase in conductivity when the pressure is lowered below the atmospheric one. Surface-adsorbed oxygen and water molecules are very effective in doping ReSe₂; hence, FETs based on this two-dimensional (2D) semiconductor can be used as an effective air pressure gauge. Finally, we report negative photoconductivity in the ReSe₂ channel that we attribute to a back-gate-dependent trapping of the photo-excited charges.

Keywords: 2D materials; rhenium; selenides; ReSe₂; field-effect transistor; pressure; negative photoconductivity



Citation: Faella, E.; Intonti, K.; Viscardi, L.; Giubileo, F.; Kumar, A.; Lam, H.T.; Anastasiou, K.; Craciun, M.F.; Russo, S.; Di Bartolomeo, A. Electric Transport in Few-Layer ReSe₂ Transistors Modulated by Air Pressure and Light. *Nanomaterials* **2022**, *12*, 1886. <https://doi.org/10.3390/nano12111886>

Academic Editor: Yun-Mo Sung

Received: 29 April 2022

Accepted: 27 May 2022

Published: 31 May 2022

Publisher's Note: MDPI stays neutral with regard to jurisdictional claims in published maps and institutional affiliations.



Copyright: © 2022 by the authors. Licensee MDPI, Basel, Switzerland. This article is an open access article distributed under the terms and conditions of the Creative Commons Attribution (CC BY) license (<https://creativecommons.org/licenses/by/4.0/>).

1. Introduction

Rhenium diselenide (ReSe₂) is a member of the layered transition metal dichalcogenides (TMDs), which has attracted a lot of attention due to the extremely anisotropic electrical, optical and mechanical properties stemming from the strong in-plane anisotropy consequence of its reduced crystal symmetry [1–4]. Contrary to other hexagonal TMDs, the room temperature thermodynamically stable 1T phase for ReSe₂ has a distorted triclinic symmetry, which endows the material with anisotropic responses in many properties [5–7].

Monolayer ReSe₂ has an indirect bandgap of 1.34 eV [8–10], reducing to 0.98 eV [6] for bulk ReSe₂, with a weak layer dependency. In general, an increase in the layer thickness causes a reduction in band-gap energy and the loss of electric properties of thick ReSe₂ [11].

ReSe₂ has been employed in various electronic and optoelectronic functional devices in order to study its electrical and optical properties. Yang et al. reported that the mobility of ReSe₂ nanosheets increases when the number of layers decreases and highlighted that the properties of ReSe₂ can be tuned by the number of layers and gas molecule gating, making ReSe₂ a promising material for future functional device applications [11]. Optically biaxial and highly anisotropic Mo-doped ReSe₂ (Mo:ReSe₂) was used to investigate the effects of physisorption of gas molecules on few-layer nanosheet-based photodetectors, reporting different sensitivity to the surrounding environment, prompt photoswitching, and high photoresponsivity [12].

The anisotropic nature of ReSe₂ was revealed by Raman spectroscopy under linearly polarized excitations in a study by Zhang et al., who fabricated top-gate ReSe₂ field-effect transistors (FETs), with a high on/off current ratio and a well-developed current saturation in the current–voltage characteristics at room temperature [7]. They synthesized

ReSe₂ directly onto hexagonal boron nitride (h-BN) substrates to improve the electron and hole mobility and demonstrated that the ReSe₂-based photodetectors exhibit polarization-sensitive photoresponsivity due to the intrinsic linear dichroism, originating from high in-plane optical anisotropy, thus, identifying ReSe₂ as a highly anisotropic two-dimensional (2D) material for novel electronic and optoelectronic applications.

Similarly, a near-infrared ReSe₂ photodetector featuring high photoresponsivity and a short photoresponse time, in the order of 10 ms, was demonstrated by Kim and coworkers, achieving high photo and temporal responses simultaneously by applying a p-doping technique based on hydrochloric acid to a selected ReSe₂ region [13].

Ambipolar FETs were obtained from multi-layer ReSe₂, mechanically exfoliated onto a SiO₂ layer by Pradhan et al., who demonstrated that it is possible to utilize the ambipolarity to fabricate logical elements or digital synthesizers [10]. Similarly, ambipolar all-2D ReSe₂ FET with a h-BN gate dielectric and graphene contacts were investigated by Lee and coworkers, who used the ambipolar transfer characteristics, attributed to the tunable Fermi level of the graphene contact, to demonstrate an inverter in a logic circuit [14].

Corbet et al. proposed a method to improve the contact resistance in few-layer ReSe₂ FETs, by up to three orders of magnitude, using ultra-high-vacuum annealing [15]. A low contact resistance was also obtained in single-layer ReSe₂, encapsulated in h-BN using scandium/gold contacts, and this enabled Khan and coworkers [16] to measure a large field-effect charge carrier mobility and responsivity.

Xing et al. addressed the challenge of the controlled synthesis of high-quality ultrathin ReSe₂, developing an approach for synthesizing 2D ReSe₂ flakes with a thickness down to monolayer by chemical vapor transport, through carefully tuning the growth kinetics [17]. The FETs fabricated with such flakes showed n-type semiconducting behavior with mobility of a few cm² V⁻¹ s⁻¹, comparable to the values measured using mechanically exfoliated flakes.

Polarization-resolved ReSe₂ photodetectors were recently studied by Tian and Liu, who reported a van der Waals heterojunction ReSe₂/WSe₂-based photodetector, with high responsivity and detectivity at room temperature. Remarkably, they demonstrated that the photoresponse of their devices is a function of the polarized angle of the incident light, indicating the effective polarized light detection [18].

Pressure is commonly used to understand the interlayer interaction in layered materials. High-hydrostatic pressures of several kbar were applied to ReSe₂ (and ReS₂) exfoliated flakes and the effect on their optical properties was investigated, finding that the energies of the two main excitonic transitions decrease in energy with increasing pressure [19]. The negative pressure coefficients were attributed to the destabilization of the p_z orbital with increasing pressure, demonstrating that ReSe₂ does not exhibit a strong electronic decoupling and, hence, the optoelectronic properties of few-layered ReSe₂ could be drastically different from the bulk form.

Conversely, the effect of low pressure on ReSe₂ has been rarely investigated in the literature.

In the present study, we fabricate back-gate FETs with a few-layer ReSe₂ channel and study the electric transport from room pressure down to 10⁻⁵ mbar. We find that air pressure has a dramatic effect on the channel conductivity, which increases by more than two orders of magnitude when the pressure decreases. We explain such behavior in terms of the desorption of oxygen and water molecules from the ReSe₂ surface in high vacuum. Importantly, we observe that the effect of air pressure is reversible, highlighting that back-gate ReSe₂ FETs can be exploited as effective pressure gauges. Moreover, we report a reduction of the channel conductivity when the device is illuminated, i.e., a negative photoconductivity, that has not been reported before for ReSe₂. The dependence of the negative photoconductivity on the gate voltage suggests that photo-excited free charge carriers are attracted towards the gate and captured at the interface, with the dielectric layer contributing to the observed loss of conductivity.

2. Materials and Methods

Ultrathin ReSe₂ flakes were exfoliated from bulk ReSe₂ single crystals using a standard mechanical exfoliation method by adhesive tape. The flakes were transferred onto highly doped n-type (resistivity 0.005 Ω cm) silicon substrates, covered by 290 nm thick SiO₂, which serves as a global back gate. Photolithography and standard lift-off process of evaporated Cr/Au (5 nm/100 nm) were applied to define metal contacts. Figure 1a reports the crystal structure and Figure 1b shows the schematic of a ReSe₂ FET with the circuit used to control the Si/SiO₂ back-gate and the source-drain bias on the 2D semiconducting channel. We adopted an interdigitated layout with 4 parallel channels corresponding to a total channel width $W = 26.0 \mu\text{m}$ and length $L = 0.78 \mu\text{m}$. An optical top view of a typical device is shown in Figure 1c. The thickness of the flake was measured by an atomic force microscope (Nanosurf AG, Liestal, Switzerland), obtaining the height profile displayed in Figure 1d that confirms a thickness of 1.84 nm, corresponding to 3 layers [20].

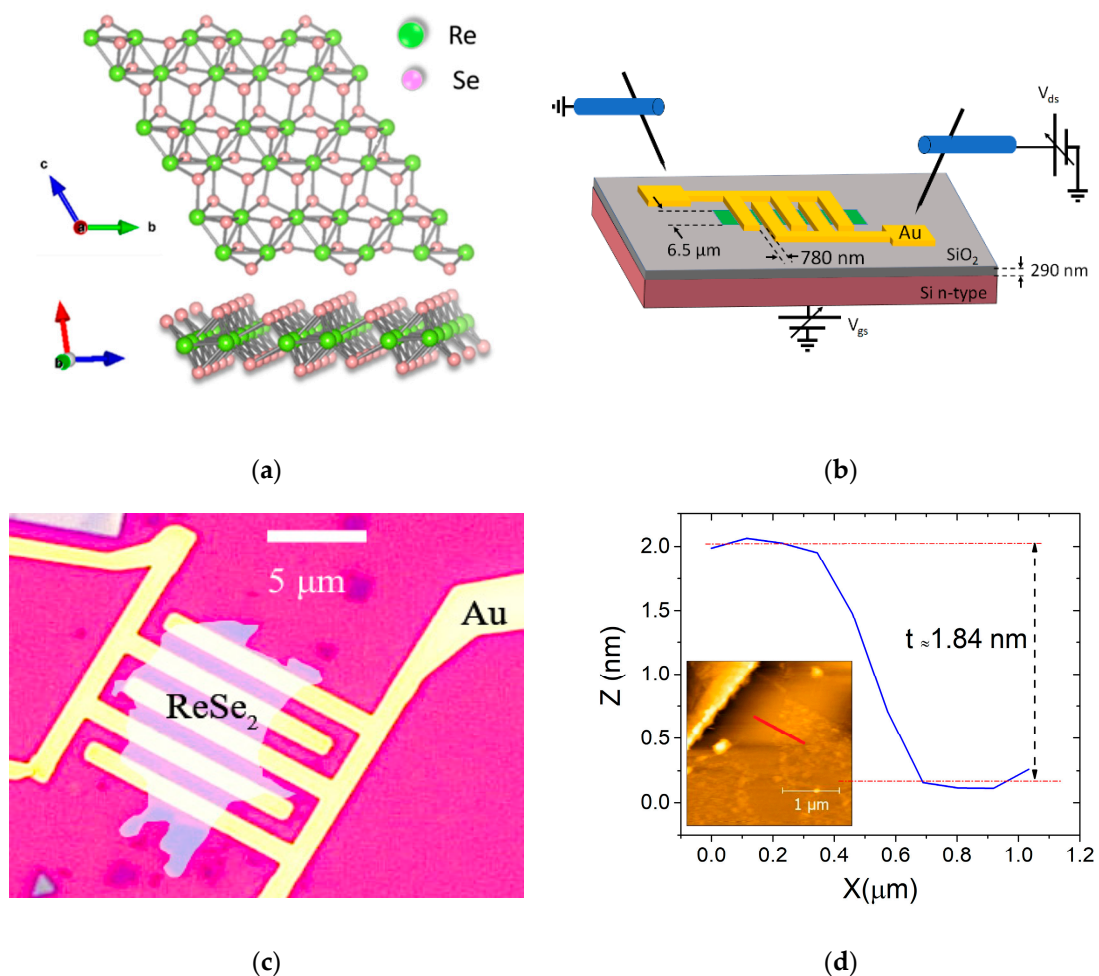


Figure 1. (a) Top view and side view of ReSe₂ atomic structure (the green and pink dots represent the Re and Se atoms, respectively); (b) schematic of the ReSe₂ back-gated FET with interdigitated source/drain leads. (c) Optical image of the ReSe₂ device with interdigitated Cr/Au leads. The flake is highlighted. (d) AFM vertical profile showing the flake thickness of 1.84 nm.

Electric measurements were carried out in two-probe configuration in a Janis ST-500 Probe Station (Lake Shore Cryotronics, Inc., Westerville, OH, USA) equipped with nanoprobe connected to the source/drain leads (Figure 1b). The back-gate voltage was applied through the sample holder of the probe station which was in direct electrical contact to the Ag-pasted n-Si substrate. The measurements were performed by the source-measurement units of a semiconductor characterization system Keithley 4200 SCS (Tek-

tronix, Inc., Beaverton, OR, USA), with current and voltage sensitivity better than 1 pA and 2 μ V, respectively. For the transistor characterization, the source was grounded while the drain (V_{ds}) and gate (V_{gs}) voltages were either swept or stepped while the drain (I_d) and gate (I_g) currents were monitored. The measured gate leakage current was always < 10 pA, confirming the integrity of the SiO₂ gate dielectric.

The electric measurements were performed at controlled air pressure, from room pressure to 10^{-5} mbar. Under the combined action of a rotatory and a turbomolecular pump connected in series to a probe station and a valve system, it was possible to control the pressure stepwise. The pressure was monitored through the pressure gauge TPG261 (Pfeiffer, Asslar, Deutschland). The photoresponse of the device was investigated using an array of 144 white LEDs with a spectrum ranging from 400 to 750 nm and peaks at 450 nm and 540 nm, a color temperature of 6000 K, and with 1 mW/cm² intensity.

3. Results and Discussion

Initially, the ReSe₂ transistor was characterized in dark and at room temperature and pressure, followed by investigating the effect of the lowering pressure in the same conditions of temperature and darkness. Finally, we explored the photoresponse of the fabricated device.

3.1. Transistor Characterization

Figure 2a,b report the output ($I_d - V_{ds}$ at fixed V_{gs}) and transfer ($I_d - V_{gs}$ at fixed V_{ds}) characteristics of the fabricated ReSe₂ FET, respectively. We limited the drain bias to 3 V and gate voltage range to ± 30 V to prevent damage to the device and, in particular, to the SiO₂ gate dielectric. The $I_d - V_{ds}$ curves (Figure 2a) show that the drain current is modulated by the gate voltage V_{gs} and stays below 10 pA for negative V_{gs} but increases abruptly for positive V_{gs} . This behavior is typical of a n-type transistor [21,22]. Furthermore, for all gate voltages, the $I_d - V_{ds}$ curves are asymmetric, with slightly higher current at positive V_{ds} , pointing to the formation of low Schottky barriers at the ReSe₂/Cr/Au contacts [23–26]. The presence of a Schottky barrier is confirmed also by the limited current that reaches the maximum of 20 nA at $V_{ds} = 3$ V.

The $I_d - V_{gs}$ transfer curves of Figure 2b, shown on both the linear and logarithmic scale, confirm the n-type behavior of the transistor, with off-state at $V_{gs} < 20$ V and on-state for $V_{gs} > 20$ V. The curve on the logarithmic scale shows an on/off current ratio higher than two orders of magnitude and a modest subthreshold swing $SS \simeq 2.8$ V/decade, typical of back-gate 2D transistors with limited gate efficiency and high interface defect density [27–30]. The smooth rise of I_d at negative V_{gs} indicates the appearance of a hole-type conduction. The carrier type can be controlled via the metal contacts. Dominant n-type behavior is obtained in ReSe₂ transistors with low-work-function metal contacts, such as Al or Ti, whose Fermi level aligns above the conduction band minimum of ReSe₂ [7,14,31]. As the conduction band minimum of ReSe₂ is around of 4.5 eV and the valence band maximum is around 5.6 eV [31], the Fermi levels of Cr and Au that have work functions of 4.5 and 5.1 eV, respectively, align within the ReSe₂ bandgap and can favor ambipolar conduction.

The transfer curve on the linear scale is used to estimate the field-effect mobility, μ_{FE} , in the on-state of the transistor for $V_{gs} > 20$ V. The mobility, evaluated as $\mu_{FE} = \frac{L}{W C_{ox} V_{ds}} \frac{dI_{ds}}{dV_{gs}}$ (here $C_{ox} = 1.15 \times 10^{-8}$ F cm⁻² is the gate dielectric capacitance per unit area), results $\mu_{FE} \simeq 0.03$ cm² V⁻¹ s⁻¹ slightly lower than the $\mu_{FE} \sim 0.1 - 10$ cm² V⁻¹ s⁻¹, typically measured in few-layer ReSe₂ FETs [5,7,10,11]. We also note that an increase in layer thickness causes a loss of electric properties in ReSe₂ and, in particular, that few-layer ReSe₂ exhibits lower mobility of two orders of magnitude or more than single-layer ReSe₂ [11]. Furthermore, the presence of a Schottky barrier at the contacts [32,33], as well as intrinsic defects in the material and impurities located at the interface with the SiO₂ layer or adsorbates on top of the channel from air exposure during the fabrication and the measurement process [10,34,35], acting as scattering or trapping centers, can contribute to decrease the mobility.

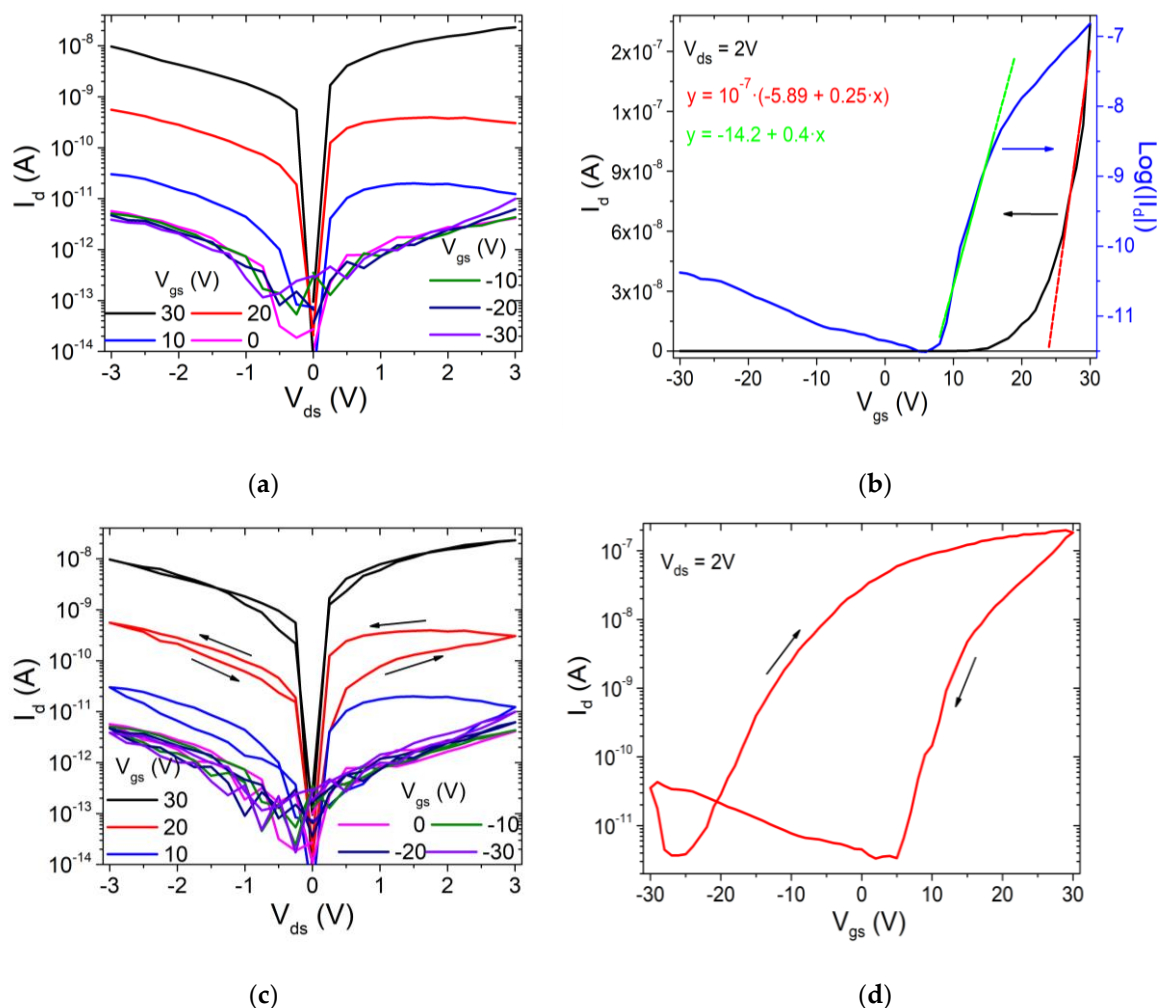


Figure 2. Electrical measurements at normal atmospheric pressure: (a) Output curves for reverse V_{ds} sweep (single). (b) Transfer curve on linear (black) and logarithmic (blue) scale. (c) Output curves for forward and reverse V_{ds} sweeps. (d) Transfer curves for forward and reverse V_{gs} sweeps, showing a wide hysteresis.

The x-axis intercept of the straight line that fits the transfer curve on the linear scale in Figure 2b is assumed as the threshold voltage V_{th} of the transistor and is about 20 V, indicating a n-type enhancement mode device.

More insights in the electric transport through the ReSe₂ channel can be gained from Figure 2c,d, which display a hysteresis on both the output and transfer curves when V_{ds} or V_{gs} are swept in a loop (the forward and reverse sweeps yield different curves). The presence of large hysteresis in the $I_d - V_{ds}$ characteristics has been reported before in monolayer MoS₂ devices, where it was attributed to the multigrain structure of the material and exploited to enable resistive switching devices. The presence of grain boundaries provides the opportunity to fabricate memristors, owing to the phenomenon of migration of defects, such as sulphur vacancies at grain boundaries, by applying a high electric field [36]. The hysteretic behavior in Figure 2c points to a defective ReSe₂ channel, possibly with Se vacancies, consistent with the n-type intrinsic doping and the low mobility. The presence of intrinsic and interfacial defects is confirmed by the huge hysteresis observed in the transfer curve in Figure 2d. Hysteresis in the transfer characteristic is very common in 2D-material-based transistors and has been widely studied and attributed to charge trapping inside the channel material, interface trap states or surface adsorbates [37,38]. The interaction with the SiO₂ dielectric, i.e., the ReSe₂/SiO₂ interface, is of paramount importance. Indeed, the substitution of the SiO₂ layer by a high-quality h-BN-insulating

substrate, which is atomically flat and free of charge trapping sites, has been shown to result in a strong mitigation of the hysteresis [39].

3.2. Pressure Behavior

To investigate the effect of air pressure on the ReSe₂ channel conductivity, we performed an electric transport measurement, lowering the atmospheric pressure down to 10⁻⁵ mbar. The measurements were performed after keeping the device at the given pressure for several hours to achieve a steady state. Figure 3a shows the output characteristics at three different pressures (room pressure, 3 mbar and 8 × 10⁻⁵ mbar) for increasing gate voltages, ranging from 0 V to 30 V, with steps of 10 V. It can be observed that the channel current increases at lower pressure while the hysteresis decreases, and the asymmetric behavior is unchanged. The reduced hysteresis indicates that surface adsorbates play an important role.

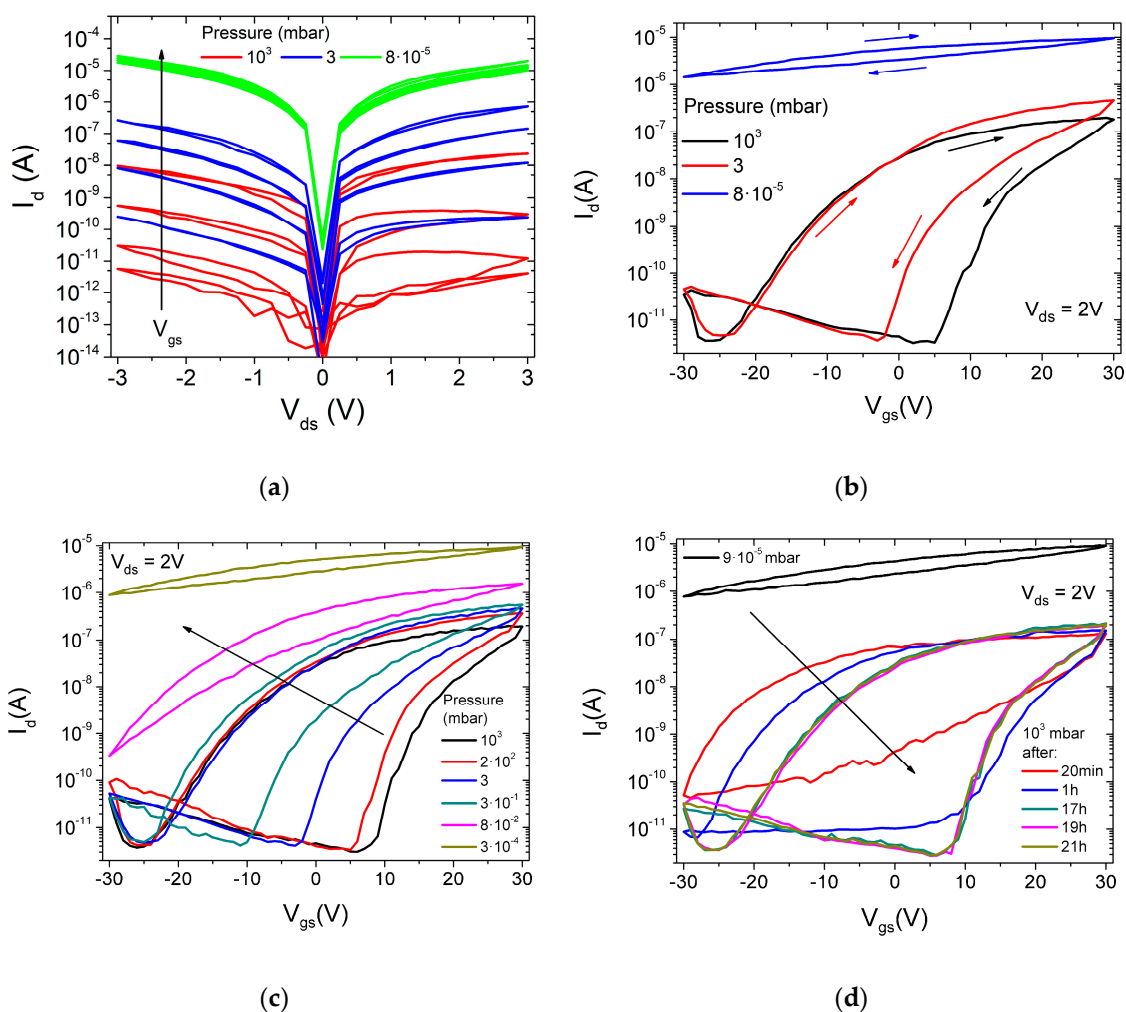


Figure 3. (a) Output curves at different gate voltages ($V_{gs} = 0, 10, 20, 30$ V) for three different air pressures (atmospheric, 3 mbar, 8 × 10⁻⁵ mbar). (b) Transfer curves for three different air pressures (atmospheric, 3 mbar, 8 × 10⁻⁵ mbar). The arrows show the direction of voltage gate sweeping starting from 30 V. Transfer characteristics (c) for lowering pressure, and (d) at different times after reaching the room pressure.

The same trend with increased current and reduced hysteresis at low pressure is displayed also by the transfer characteristics in Figure 3b. The low pressure, in particular, causes a dramatic change in the transfer characteristics with the transistor that does not turn off over the applied V_{gs} range. The lowering pressure causes a left shift in the transfer

characteristics, corresponding to a reduction in the threshold voltage V_{th} , pointing to an increased n-type doping density. Such behavior can be explained as desorption of adsorbates from the ReSe₂ surface. Adsorbed oxygen and water molecules, being electronegative, subtract electrons to the channel, thus, decreasing the conductivity (otherwise stated, oxygen and water counter-dope the n-type channel with holes). Their desorption has the two-fold beneficial effect of increasing the n-type doping and the mobility (see following), resulting in increased conductivity.

Figure 3c,d, which display the transfer characteristics for lowering and raising pressures, respectively, demonstrate that the transformation of the transfer curves is gradual and reversible. While the plot in Figure 3c shows the dynamic evolution of the transfer curves during the pressure change, the plot in Figure 3d monitors the time evolution of the transfer curves after a sudden change from 8×10^{-5} mbar to room pressure, showing that the recovery of the pristine state is a slow process, requiring a few hours. The reversible change of current with pressure demonstrates that the device can be used as an air pressure gauge.

Figure 4a,b detail the behavior of the mobility μ_{FE} and of the current in the on state (I_{on}) as a function of pressure. The mobility was evaluated using both the forward (V_{gs} sweep from -30 V to 30 V) and reverse (V_{gs} sweep from 30 V to -30 V) branches of transfer characteristics. Both forward μ_{FE} and I_{on} decrease for increasing pressure, following a power law, as demonstrated by the linear log–log plots in the respective insets. Conversely, the threshold voltage V_{th} increases up to 10^{-1} mbar, above which it reaches a plateau (Figure 4c), demonstrating that the desorption of the adsorbates becomes effective at a pressure below 10^{-1} mbar. Finally, Figure 4d shows that the hysteresis width (here defined as the difference between the V_{gs} corresponding to the current $I_d = 1$ nA in the reverse and forward sweep) is also increased by the rising pressure. The contribution of adsorbates to hysteresis in 2D-material-based transistors has been widely studied and demonstrated [34,40,41]. The easier the charge transfer between the channel and the adsorbates, the wider the hysteresis [38].

3.3. Photoresponse

As ReSe₂ nanosheets have been widely used in efficient photodetectors [7,13,42], we checked the photoresponse of the ReSe₂ FET by exposing it to the light of an array of white LEDs at a pressure of 8×10^{-5} mbar.

Figure 5a shows that the current I_d decreases when the device is illuminated, a phenomenon referred to as negative photoconductivity. The decrease in the current under light is enhanced at $V_{gs} = 30$ V. Illumination normally generates additional carriers in a semiconductor material, which increase its conductivity. Conversely, negative photoconductivity has been reported in a few 1D and 2D materials, and explained as a photogating effect due to trap centers, light-induced desorption of surface gas molecules or surface plasmons [43–47]. The origin and role of the negative photoconductivity in low-dimensional materials is still poorly understood. Moreover, negative photoconductivity has not been observed before in ReSe₂ and requires deep investigation that will be the subject of a forthcoming study. Here, we note that the photocurrent ($I_{ph} = I_{light} - I_{dark}$) increases with the drain bias and has the absolute value tunable by the gate voltage, as shown in Figure 5b. The increase in the photocurrent with V_{ds} is easily understood because a higher horizontal field favors charge collection to the drain. The increasing $|I_{ph}|$ with the higher gate bias instead suggests a mechanism for the negative photoconductivity, as gate-induced photo-excited charges separation and trapping. The photogenerated electron-hole pairs are separated by the vertical gate field, which attracts electrons at the ReSe₂/SiO₂ interface, where they become trapped. The excess holes in the channels combine with electrons of the n-type ReSe₂, causing a counter-doping effect, i.e., a reduction in the channel conductivity.

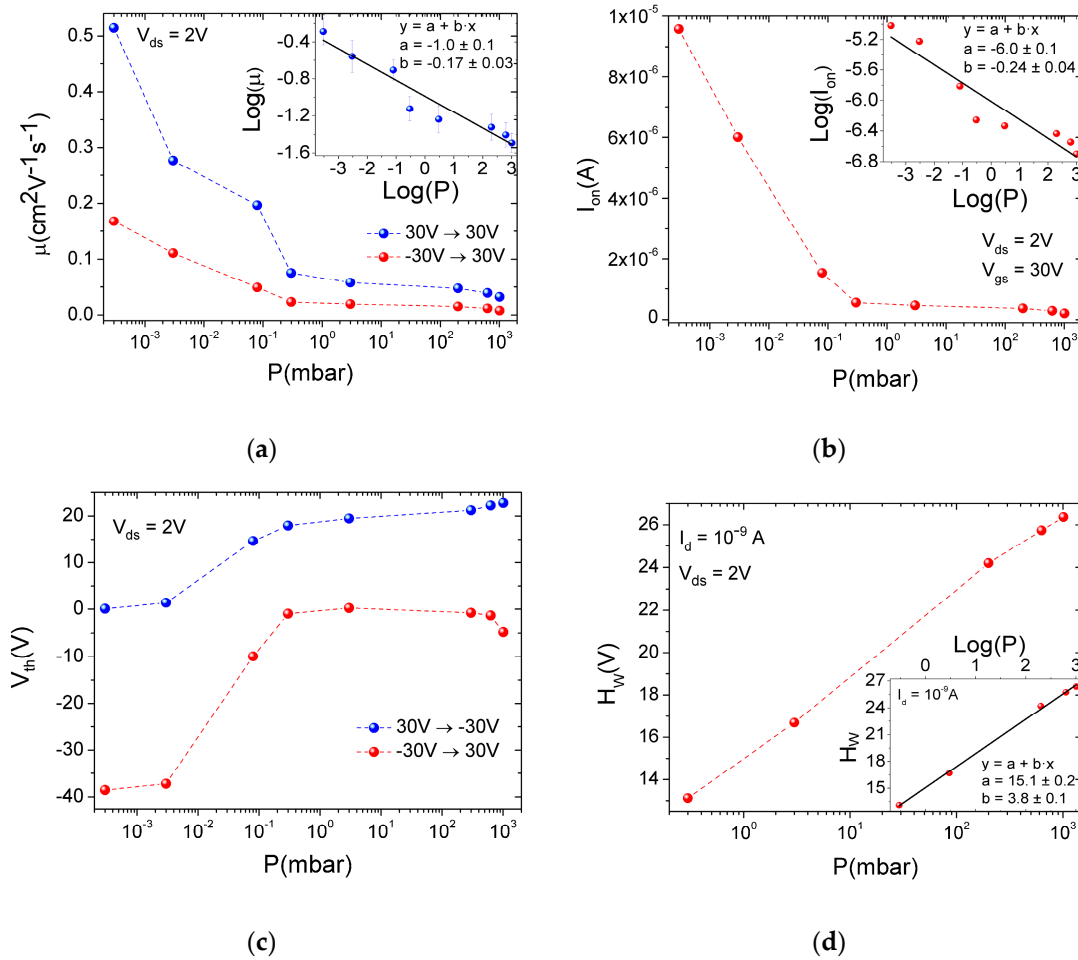


Figure 4. (a) Forward and reverse mobility as function of pressure. Linear fit of the data on log–log scale in the inset, (b) current in the on state as function of pressure. Linear fit of the data on log–log scale in inset, (c) forward and reverse threshold voltage as function of pressure, and (d) hysteresis width at $I_d = 1\text{ nA}$ versus air pressure. Linear fit of data on semi-log scale in the inset.

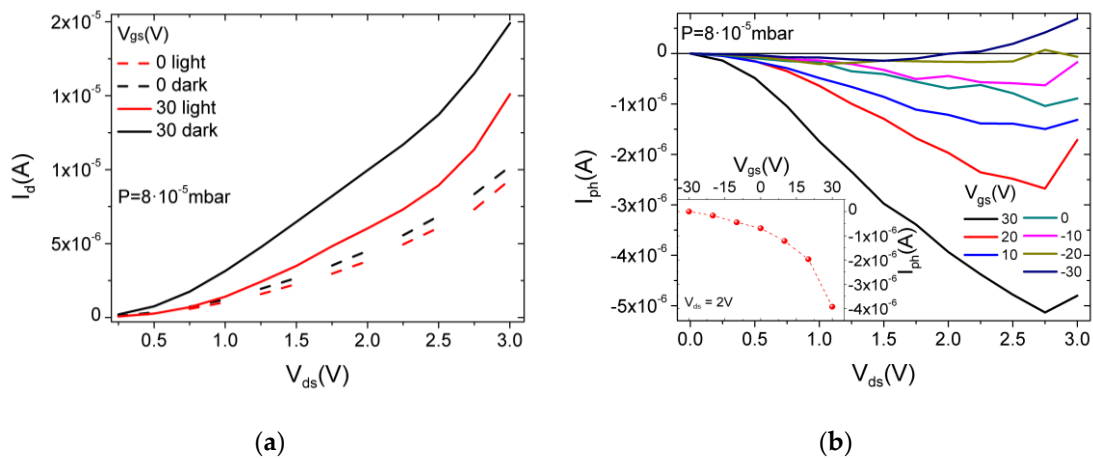


Figure 5. (a) $I_{\text{ds}} - V_{\text{ds}}$ curves in dark and light at $V_{\text{gs}} = 0$ and $+30\text{V}$ (dashed and solid lines); (b) $I_{\text{ph}} - V_{\text{ds}}$ curves at different V_{gs} . I_{ph} vs. V_{gs} at $V_{\text{ds}} = 2\text{V}$ in the inset.

4. Conclusions

We fabricated a back-gate field-effect transistor with ReSe₂ nanosheets and Cr/Au contacts and studied its electric transport. We showed that the transistor has a dominant n-type character due to the alignment of the Cr Fermi level with the ReSe₂ conduction band minimum. We investigated the effect of low pressure on the material conductivity and found that the device is strongly affected by air pressure. The exposure to air suppresses the channel conductivity as an effect of electron capture by oxygen and water molecules adsorbed on the material surface. The desorption of adsorbates in high vacuum increases the channel conductivity. We pointed out that the reversible pressure behavior allows the device to be used as an air pressure gauge. Furthermore, we showed that the n-type channel and the gate-driven separation and trapping of photogenerated electrons can lower the channel conductivity under illumination, the origin of the observed negative photoconductivity.

Author Contributions: Conceptualization, S.R. and A.D.B.; methodology, H.T.L., M.F.C., E.F., F.G. and K.A.; software, E.F., K.I., A.K. and L.V.; validation, A.D.B., M.F.C., F.G. and S.R.; formal analysis, E.F., K.I. and L.V.; investigation, E.F., K.I., L.V., H.T.L., K.A. and A.K.; resources, S.R. and A.D.B.; data curation, E.F., K.I., L.V. and A.K.; writing—original draft preparation, A.D.B. and E.F.; writing—review and editing, A.D.B., F.G., M.F.C. and S.R.; visualization, E.F., K.I., H.T.L. and K.A.; supervision, A.D.B. and S.R.; project administration, A.D.B., M.F.C. and S.R.; funding acquisition, F.G. and M.F.C. All authors have read and agreed to the published version of the manuscript.

Funding: This research was funded by the University of Salerno, Italy, grant number ORSA218189 and ORSA200207. The APC was funded by A.D.B.

Institutional Review Board Statement: Not applicable.

Informed Consent Statement: Not applicable.

Data Availability Statement: The data presented in this study are available on request from the corresponding author.

Conflicts of Interest: The authors declare no conflict of interest.

References

1. Friemelt, K.; Lux-Steiner, M.C.; Bucher, E. Optical Properties of the Layered Transition-Metal-Dichalcogenide ReS₂: Anisotropy in the van Der Waals Plane. *J. Appl. Phys.* **1993**, *74*, 5266–5268. [[CrossRef](#)]
2. Ho, C.H.; Huang, C.E. Optical Property of the Near Band-Edge Transitions in Rhenium Disulfide and Diselenide. *J. Alloys Compd.* **2004**, *383*, 74–79. [[CrossRef](#)]
3. Dumcenco, D.O.; Huang, W.Y.; Huang, Y.S.; Tiong, K.K. Anisotropic Optical Characteristics of Au-Doped Rhenium Diselenide Single Crystals. *J. Alloys Compd.* **2009**, *480*, 104–106. [[CrossRef](#)]
4. Di Bartolomeo, A. Emerging 2D Materials and Their Van Der Waals Heterostructures. *Nanomaterials* **2020**, *10*, 579. [[CrossRef](#)] [[PubMed](#)]
5. Cui, F.; Li, X.; Feng, Q.; Yin, J.; Zhou, L.; Liu, D.; Liu, K.; He, X.; Liang, X.; Liu, S.; et al. Epitaxial Growth of Large-Area and Highly Crystalline Anisotropic ReSe₂ Atomic Layer. *Nano Res.* **2017**, *10*, 2732–2742. [[CrossRef](#)]
6. Ho, C.H.; Huang, Y.S.; Tiong, K.K. In-Plane Anisotropy of the Optical and Electrical Properties of ReS₂ and ReSe₂ Layered Crystals. *J. Alloy. Compd.* **2001**, *317*, 222–226. [[CrossRef](#)]
7. Zhang, E.; Wang, P.; Li, Z.; Wang, H.; Song, C.; Huang, C.; Chen, Z.-G.; Yang, L.; Zhang, K.; Lu, S.; et al. Tunable Ambipolar Polarization-Sensitive Photodetectors Based on High-Anisotropy ReSe₂ Nanosheets. *ACS Nano* **2016**, *10*, 8067–8077. [[CrossRef](#)]
8. Wolverson, D.; Crampin, S.; Kazemi, A.S.; Ilie, A.; Bending, S.J. Raman Spectra of Monolayer, Few-Layer, and Bulk ReSe₂: An Anisotropic Layered Semiconductor. *ACS Nano* **2014**, *8*, 11154–11164. [[CrossRef](#)]
9. Hart, L.S.; Webb, J.L.; Dale, S.; Bending, S.J.; Mucha-Kruczynski, M.; Wolverson, D.; Chen, C.; Avila, J.; Asensio, M.C. Electronic Bandstructure and van Der Waals Coupling of ReSe₂ Revealed by High-Resolution Angle-Resolved Photoemission Spectroscopy. *Sci. Rep.* **2017**, *7*, 5145. [[CrossRef](#)]
10. Pradhan, N.R.; Garcia, C.; Isenberg, B.; Rhodes, D.; Feng, S.; Memaran, S.; Xin, Y.; McCreary, A.; Walker, A.R.H.; Raelarijaona, A.; et al. Phase Modulators Based on High Mobility Ambipolar ReSe₂ Field-Effect Transistors. *Sci. Rep.* **2018**, *8*, 12745. [[CrossRef](#)]
11. Yang, S.; Tongay, S.; Li, Y.; Yue, Q.; Xia, J.-B.; Li, S.-S.; Li, J.; Wei, S.-H. Layer-Dependent Electrical and Optoelectronic Responses of ReSe₂ Nanosheet Transistors. *Nanoscale* **2014**, *6*, 7226. [[CrossRef](#)] [[PubMed](#)]

12. Yang, S.; Tongay, S.; Yue, Q.; Li, Y.; Li, B.; Lu, F. High-Performance Few-Layer Mo-Doped ReSe₂ Nanosheet Photodetectors. *Sci. Rep.* **2015**, *4*, 5442. [[CrossRef](#)] [[PubMed](#)]
13. Kim, J.; Heo, K.; Kang, D.; Shin, C.; Lee, S.; Yu, H.; Park, J. Rhenium Diselenide (ReSe₂) Near-Infrared Photodetector: Performance Enhancement by Selective P-Doping Technique. *Adv. Sci.* **2019**, *6*, 1901255. [[CrossRef](#)] [[PubMed](#)]
14. Lee, K.; Yang, S.; Sung, Y.; Chang, Y.; Lin, C.; Yang, F.; Li, M.; Watanabe, K.; Taniguchi, T.; Ho, C.; et al. Analog Circuit Applications Based on All-2D Ambipolar ReSe₂ Field-Effect Transistors. *Adv. Funct. Mater.* **2019**, *29*, 1809011. [[CrossRef](#)]
15. Corbet, C.M.; Sonde, S.S.; Tutuc, E.; Banerjee, S.K. Improved Contact Resistance in ReSe₂ Thin Film Field-Effect Transistors. *Appl. Phys. Lett.* **2016**, *108*, 162104. [[CrossRef](#)]
16. Khan, M.F.; Rehman, S.; Akhtar, I.; Aftab, S.; Ajmal, H.M.S.; Khan, W.; Kim, D.; Eom, J. High Mobility ReSe₂ Field Effect Transistors: Schottky-Barrier-Height-Dependent Photoresponsivity and Broadband Light Detection with Co Decoration. *2D Mater.* **2019**, *7*, 015010. [[CrossRef](#)]
17. Xing, L.; Yan, X.; Zheng, J.; Xu, G.; Lu, Z.; Liu, L.; Wang, J.; Wang, P.; Pan, X.; Jiao, L. Highly Crystalline ReSe₂ Atomic Layers Synthesized by Chemical Vapor Transport. *InfoMat* **2019**, *1*, 552–558. [[CrossRef](#)]
18. Tian, X.; Liu, Y. Van Der Waals Heterojunction ReSe₂/WSe₂ Polarization-Resolved Photodetector. *J. Semicond.* **2021**, *42*, 032001. [[CrossRef](#)]
19. Oliva, R.; Laurien, M.; Dybala, F.; Kopaczek, J.; Qin, Y.; Tongay, S.; Rubel, O.; Kudrawiec, R. Pressure Dependence of Direct Optical Transitions in ReS₂ and ReSe₂. *Npj 2D Mater. Appl.* **2019**, *3*, 20. [[CrossRef](#)]
20. Tongay, S.; Sahin, H.; Ko, C.; Luce, A.; Fan, W.; Liu, K.; Zhou, J.; Huang, Y.-S.; Ho, C.-H.; Yan, J.; et al. Monolayer Behavior in Bulk ReS₂ Due to Electronic and Vibrational Decoupling. *Nat. Commun.* **2014**, *5*, 3252. [[CrossRef](#)]
21. Di Bartolomeo, A.; Urban, F.; Passacantando, M.; McEvoy, N.; Peters, L.; Iemmo, L.; Luongo, G.; Romeo, F.; Giubileo, F. A WSe₂ Vertical Field Emission Transistor. *Nanoscale* **2019**, *11*, 1538–1548. [[CrossRef](#)] [[PubMed](#)]
22. Urban, F.; Martucciello, N.; Peters, L.; McEvoy, N.; Di Bartolomeo, A. Environmental Effects on the Electrical Characteristics of Back-Gated WSe₂ Field-Effect Transistors. *Nanomaterials* **2018**, *8*, 901. [[CrossRef](#)] [[PubMed](#)]
23. Grillo, A.; Di Bartolomeo, A. A Current–Voltage Model for Double Schottky Barrier Devices. *Adv. Electron. Mater.* **2021**, *7*, 2000979. [[CrossRef](#)]
24. Di Bartolomeo, A.; Grillo, A.; Urban, F.; Iemmo, L.; Giubileo, F.; Luongo, G.; Amato, G.; Croin, L.; Sun, L.; Liang, S.-J.; et al. Asymmetric Schottky Contacts in Bilayer MoS₂ Field Effect Transistors. *Adv. Funct. Mater.* **2018**, *28*, 1800657. [[CrossRef](#)]
25. Ezhilmaran, B.; Patra, A.; Benny, S.; Sreelakshmi, M.R.; Akshay, V.V.; Bhat, S.V.; Rout, C.S. Recent Developments in the Photodetector Applications of Schottky Diodes Based on 2D Materials. *J. Mater. Chem. C* **2021**, *9*, 6122–6150. [[CrossRef](#)]
26. Giubileo, F.; Di Bartolomeo, A. The Role of Contact Resistance in Graphene Field-Effect Devices. *Prog. Surf. Sci.* **2017**, *92*, 143–175. [[CrossRef](#)]
27. Pelella, A.; Grillo, A.; Urban, F.; Giubileo, F.; Passacantando, M.; Pollmann, E.; Sleziona, S.; Schleberger, M.; Di Bartolomeo, A. Gate-Controlled Field Emission Current from MoS₂ Nanosheets. *Adv. Electron. Mater.* **2021**, *7*, 2000838. [[CrossRef](#)]
28. Di Bartolomeo, A.; Pelella, A.; Urban, F.; Grillo, A.; Iemmo, L.; Passacantando, M.; Liu, X.; Giubileo, F. Field Emission in Ultrathin PdSe₂ Back-Gated Transistors. *Adv. Electron. Mater.* **2020**, *6*, 2000094. [[CrossRef](#)]
29. Sun, J.; Passacantando, M.; Palummo, M.; Nardone, M.; Kaasbjerg, K.; Grillo, A.; Di Bartolomeo, A.; Caridad, J.M.; Camilli, L. Impact of Impurities on the Electrical Conduction of Anisotropic Two-Dimensional Materials. *Phys. Rev. Appl.* **2020**, *13*, 044063. [[CrossRef](#)]
30. Di Bartolomeo, A.; Urban, F.; Pelella, A.; Grillo, A.; Iemmo, L.; Faella, E.; Giubileo, F. Electrical Transport in Two-Dimensional PdSe₂ and MoS₂ Nanosheets. In Proceedings of the 2020 IEEE 20th International Conference on Nanotechnology (IEEE-NANO), Montreal, QC, Canada, 28–31 July 2020; pp. 276–281.
31. Kang, B.; Kim, Y.; Cho, J.H.; Lee, C. Ambipolar Transport Based on CVD-Synthesized ReSe₂. *2D Mater.* **2017**, *4*, 025014. [[CrossRef](#)]
32. Urban, F.; Lupina, G.; Grillo, A.; Martucciello, N.; Di Bartolomeo, A. Contact Resistance and Mobility in Back-Gate Graphene Transistors. *Nano Express* **2020**, *1*, 010001. [[CrossRef](#)]
33. Pelella, A.; Kharsah, O.; Grillo, A.; Urban, F.; Passacantando, M.; Giubileo, F.; Iemmo, L.; Sleziona, S.; Pollmann, E.; Madauß, L.; et al. Electron Irradiation of Metal Contacts in Monolayer MoS₂ Field-Effect Transistors. *ACS Appl. Mater. Interfaces* **2020**, *12*, 40532–40540. [[CrossRef](#)] [[PubMed](#)]
34. Di Bartolomeo, A.; Genovese, L.; Giubileo, F.; Iemmo, L.; Luongo, G.; Foller, T.; Schleberger, M. Hysteresis in the Transfer Characteristics of MoS₂ Transistors. *2D Mater.* **2017**, *5*, 015014. [[CrossRef](#)]
35. Giubileo, F.; Iemmo, L.; Passacantando, M.; Urban, F.; Luongo, G.; Sun, L.; Amato, G.; Enrico, E.; Di Bartolomeo, A. Effect of Electron Irradiation on the Transport and Field Emission Properties of Few-Layer MoS₂ Field-Effect Transistors. *J. Phys. Chem. C* **2019**, *123*, 1454–1461. [[CrossRef](#)]
36. Sangwan, V.K.; Jariwala, D.; Kim, I.S.; Chen, K.-S.; Marks, T.J.; Lauhon, L.J.; Hersam, M.C. Gate-Tunable Memristive Phenomena Mediated by Grain Boundaries in Single-Layer MoS₂. *Nat. Nanotechnol.* **2015**, *10*, 403–406. [[CrossRef](#)] [[PubMed](#)]
37. Di Bartolomeo, A.; Pelella, A.; Liu, X.; Miao, F.; Passacantando, M.; Giubileo, F.; Grillo, A.; Iemmo, L.; Urban, F.; Liang, S. Pressure-Tunable Ambipolar Conduction and Hysteresis in Thin Palladium Diselenide Field Effect Transistors. *Adv. Funct. Mater.* **2019**, *29*, 1902483. [[CrossRef](#)]
38. Urban, F.; Giubileo, F.; Grillo, A.; Iemmo, L.; Luongo, G.; Passacantando, M.; Foller, T.; Madauß, L.; Pollmann, E.; Geller, M.P.; et al. Gas Dependent Hysteresis in MoS₂ Field Effect Transistors. *2D Mater.* **2019**, *6*, 045049. [[CrossRef](#)]

39. Lee, C.; Rathi, S.; Khan, M.A.; Lim, D.; Kim, Y.; Yun, S.J.; Youn, D.-H.; Watanabe, K.; Taniguchi, T.; Kim, G.-H. Comparison of Trapped Charges and Hysteresis Behavior in HBN Encapsulated Single MoS₂ Flake Based Field Effect Transistors on SiO₂ and HBN Substrates. *Nanotechnology* **2018**, *29*, 335202. [[CrossRef](#)]
40. Knobloch, T.; Rzepa, G.; Illarionov, Y.Y.; Waltl, M.; Schanovsky, F.; Stampfer, B.; Furchi, M.M.; Mueller, T.; Grasser, T. A Physical Model for the Hysteresis in MoS₂ Transistors. *IEEE J. Electron Devices Soc.* **2018**, *6*, 972–978. [[CrossRef](#)]
41. Shu, J.; Wu, G.; Guo, Y.; Liu, B.; Wei, X.; Chen, Q. The Intrinsic Origin of Hysteresis in MoS₂ Field Effect Transistors. *Nanoscale* **2016**, *8*, 3049–3056. [[CrossRef](#)]
42. Silva, B.; Rodrigues, J.; Sompalle, B.; Liao, C.-D.; Nicoara, N.; Borme, J.; Cerqueira, F.; Claro, M.; Sadewasser, S.; Alpuim, P.; et al. Efficient ReSe₂ Photodetectors with CVD Single-Crystal Graphene Contacts. *Nanomaterials* **2021**, *11*, 1650. [[CrossRef](#)] [[PubMed](#)]
43. Han, Y.; Zheng, X.; Fu, M.; Pan, D.; Li, X.; Guo, Y.; Zhao, J.; Chen, Q. Negative Photoconductivity of InAs Nanowires. *Phys. Chem. Chem. Phys.* **2016**, *18*, 818–826. [[CrossRef](#)] [[PubMed](#)]
44. Di Bartolomeo, A.; Urban, F.; Faella, E.; Grillo, A.; Pelella, A.; Giubileo, F.; Askari, M.B.; McEvoy, N.; Gity, F.; Hurley, P.K. PtSe₂ Phototransistors with Negative Photoconductivity. *J. Phys. Conf. Ser.* **2021**, *1866*, 012001. [[CrossRef](#)]
45. Urban, F.; Gity, F.; Hurley, P.K.; McEvoy, N.; Di Bartolomeo, A. Isotropic Conduction and Negative Photoconduction in Ultrathin PtSe₂ Films. *Appl. Phys. Lett.* **2020**, *117*, 193102. [[CrossRef](#)]
46. Grillo, A.; Faella, E.; Pelella, A.; Giubileo, F.; Ansari, L.; Gity, F.; Hurley, P.K.; McEvoy, N.; Di Bartolomeo, A. Coexistence of Negative and Positive Photoconductivity in Few-Layer PtSe₂ Field-Effect Transistors. *Adv. Funct. Mater.* **2021**, *31*, 2105722. [[CrossRef](#)]
47. Cui, B.; Xing, Y.; Han, J.; Lv, W.; Lv, W.; Lei, T.; Zhang, Y.; Ma, H.; Zeng, Z.; Zhang, B. Negative Photoconductivity in Low-Dimensional Materials. *Chin. Phys. B* **2021**, *30*, 028507. [[CrossRef](#)]